Molecular Design and In Situ Spectroscopic Investigation of Multilayered Supported $M_1Ox/M_2Ox/SiO_2$ Catalysts

Edward L. Lee and Israel E. Wachs*

Operando Molecular Spectroscopy and Catalysis Laboratory, Chemical Engineering Department, 111 Research Drive, Iacocca Hall, Lehigh University, Bethlehem, Pennsylvania 18015

Received: June 16, 2008; Revised Manuscript Received: October 16, 2008

The group 5−7 transition metal oxides (V_2O_5, CrO_3, MoO_3, WO_3, and Re_2O_7) were anchored on a surface modified SiO_2 support containing surface alumina, zirconia, and titania species prepared via incipient wetness impregnation of soluble precursors and calcination. The molecular and electronic structures of these "multilayered" supported $M_1Ox/M_2Ox/SiO_2$ catalysts were characterized with in situ Raman and UV−vis DRS spectroscopies under dehydrated conditions to provide insights into the interactions between the metal oxide overlayer (M_1Ox) and the surface oxide modifiers (M_2Ox) on the silica support. The supported M_1Ox transition metal oxides preferentially coordinate to the surface M_2Ox modifiers over exposed SiO_2 support sites and are present as isolated surface M_1Ox species. Although the molecular and electronic structures of monoxo surface $O{=}VO_3$ and trioxo surface $(O{=})_3ReO$ species are not appreciably perturbed by the surface modifiers, the group 6 surface CrOx, MoOx and WOx species are significantly altered by the presence of the surface M_2Ox additives. The monoxo $[O{=}MO_4]$/dioxo $[(O{=})_2MO_2]$ ratio of the silica-supported group 6 metal oxides is found to be controlled by the surface modifiers. The electronic structures of the group 6 surface metal oxides exhibit fewer LMCT transitions in the UV−vis spectra and higher Eg values in the presence of the surface M_2Ox modifiers. Thus, both the molecular and electronic structures of the dehydrated group 6 surface metal oxides on SiO_2 supports can be *tuned* with the addition of surface oxide modifiers.

1. Introduction

Supported metal oxide catalysts consist of an active metal oxide phase deposited on a high surface area oxide support (SiO_2, Al_2O_3, TiO_2, etc.) and find use for numerous catalyzed reactions in the chemical, petroleum and environmental industries.[1−3] The supported metal oxide phase below monolayer surface coverage or maximum dispersion limits is present as a two-dimensional surface metal oxide layer that is 100% dispersed on the support and terminates with different functional groups such as M−O$^-$, M−OH, M−O−M, or M═O.[4−9] The dehydrated transition metal oxides of the groups 5−7 possess unique molecular structures since they have been shown to terminate with monoxo (M═O), dioxo (M(═O)$_2$), or trioxo (M(═O)$_3$) functionalities.[9] Extensive in situ Raman, IR, and UV−vis spectroscopic characterization under various environments (dehydrated, oxidizing, reducing, and D_2O-H_2O and $^{18}O-^{16}O$ isotopic exchange) have been undertaken to determine the molecular and electronic structures of the supported group 5−7 surface metal oxides on SiO_2.[10,11] The group 5 silica-supported metal oxides solely consist of isolated surface monoxo $O{=}M(-O-Si)_3$ species,[12−14] the group 6 silica-supported metal oxides predominantly possess isolated surface dioxo $(O{=})_2M(-O-Si)_2$ species and to a lesser extent isolated surface $O{=}M(-O-Si)_4$ species,[15−18] and the group 7 silica-supported metal oxide system of rhenium oxide consisting of isolated surface trioxo $(O{=})_3M-O-Si$ species.[10,11]

Various surface modifiers or additives are generally introduced to the supported MOx/SiO_2 catalyst systems to enhance their catalytic performance (higher activity, higher selectivity, higher surface area, etc.). Some typical additives are surface oxides of AlOx, ZrOx, and TiOx. The interaction between $Al_2O_3-SiO_2$ generates new Brønsted acidic sites at the bridging Al−OH−Si bond,[19] the ZrO_2-SiO_2 interaction results in surface acidity, excellent chemical resistance to alkaline corrosion as well as low thermal expansion,[20] and the interaction between TiO_2-SiO_2 yields high thermal stability, excellent mechanical strength, as well as the generation of new catalytic active and acidic sites.[21] These surface modified SiO_2 materials are then used as oxide supports for the group 5−7 transition metal oxides. The literature reports various industrial applications for these silica-supported oxide catalysts: ammoxidation of 3-picoline ($V_2O_5/Al_2O_3-SiO_2$),[22] selective catalytic reduction (SCR) of nitrogen oxide with ammonia and NO reduction with CO ($V_2O_5/TiO_2/SiO_2$),[23−27] oxidative dehydrogenation of various alkanes and alcohols (V_2O_5/TiO_2-SiO_2),[28−30] ethylene polymerization (CrO_3/TiO_2-SiO_2),[31,32] hydrodenitrogenation (HDN) of nitrogen containing heteroaromatic compounds ($Mo/Al_2O_3-SiO_2$).[33,34] hydrodesulfurization (HDS) of thiophene and other compounds (Mo/ZrO_2-SiO_2 and MoO_3/TiO_2-SiO_2),[35−37] alkene metathesis and epoxidation with H_2O_2 ($Re_2O_7/Al_2O_3-SiO_2$).[38,39] These SiO_2 promoted mixed oxide support materials have favorable catalytic properties over the more conventional supported MOx/SiO_2 catalysts. The influence of the surface AlOx, ZrOx, and TiOx additives on the molecular and electronic structures of the supported group 5−7 transition metal oxides for silica-supported catalysts, however, has received incomplete attention with exception of the supported vanadia systems.[19−21,40−44] Such fundamental structural information is critical for understanding the catalytic properties of surface modified SiO_2-supported group 5−7 transition metal oxides.

The present study examines the influence of surface modified SiO_2 supports (e.g., $AlOx/SiO_2$, $ZrOx/SiO_2$, and $TiOx/SiO_2$) on the surface structures of the dispersed group 5−7 transition metal

* To whom correspondence should be addressed. E-mail: iew0@lehigh.edu. Phone: (610) 758-4274. Fax: (610) 758-6555.

10.1021/jp805265m CCC: $40.75
Published on Web 12/02/2008

oxide (V_2O_5, CrO_3, MoO_3, WO_3, Re_2O_7) catalytic active sites ("multilayered catalysts"). The molecular and electronic structures of the surface group 5−7 metal oxides will be determined with in situ Raman and UV−vis diffuse reflectance spectroscopy (DRS), respectively, under oxidizing conditions where the catalysts are in a dehydrated state.[1−3] In situ Raman provides molecular structural information about the surface MOx species by establishing the number of terminal M═O bonds. Complementary in situ UV−vis DRS further examines the local structure (isolated monomers, dimers, polymeric chains, etc.) of the surface MOx species via the ligand-to-metal charge transfer (LMCT) band and its corresponding edge energy (Eg) value.[2,9] The influence of the surface modified SiO_2 support upon the number of terminal M═O bonds for each surface metal oxide system and their local structures will be examined. It is found that the molecular and electronic structures of the supported group 5−7 transition metal oxides are altered by the surface alumina, zirconia, and titania ligands. The surface structures of the supported group 5−7 metal oxides on the surface modified SiO_2 will only be presented in this paper and the corresponding catalytic properties are described in a subsequent paper.[45] The combination of the structural and catalytic performance information will allow for the establishment of fundamental structure−activity relationships of such multilayered catalyst systems.

2. Experimental Methods

2.1. Catalyst Synthesis. The silica-supported catalysts consist of highly dispersed metal oxides (Al_2O_3, TiO_2, ZrO_2, V_2O_5, CrO_3, MoO_3, WO_3, and Re_2O_7) that were successfully prepared by incipient wetness impregnation, further detailed elsewhere.[46−48] The silica support material, amorphous SiO_2 (Cabot, Cab-O-Sil fumed silica EH-5, S.A. = 332 m^2/g), was employed and found to be more easily handled by an initial water pretreatment and calcination at 500 °C for 4 h without changing the material properties. The silica support was impregnated with aqueous or nonaqueous (toluene) solutions of the corresponding precursors: aluminum sec-butoxide ($Al[O(CH_3)CH_2H_5]_3$, Alfa Aesar, 95%), titanium isopropoxide ($Ti[OCH(CH_3)_2]_4$, Alfa-Aesar, 99.999%), or zirconium tert-butoxide ($Zr[OC(CH_3)_3]_4$, Alfa Aesar, 97%), vanadium triisopropoxide ($VO[CHO(CH_3)_2]_3$, Alfa Aesar, 97%), chromium(III) nitrate ($Cr(NO_3)_3 \cdot 9H_2O$, Alfa Aesar, 98.5%), ammonium heptamolybdate ($(NH_4)_6Mo_7O_{24} \cdot 4H_2O$, Aldrich, 99.98%), ammonium metatungstate ($(NH_4)_6H_2W_{12}O_{40} \cdot xH_2O$, Pfaltz and Bauer, 99.5%), and perrhenic acid ($HReO_4$, Alfa Aesar, 75−80%). The silica was initially dried for 2 h at 115 °C for the nonaqueous preparations prior to surface modification inside a glovebox (Vacuum Atmospheres, Omni-Laboratory VAC 101965) under nitrogen environments. After impregnation, the samples were allowed to dry overnight under the nitrogen atmosphere. The calcination of the samples entailed ramping at 1 °C/min to 110 °C and held for 5 h under flowing N_2 (Airgas, Ultra High Purity) in a programmable furnace (Thermolyne, Model 48000), subsequently followed by another 1 °C/min ramp under flowing air (Airgas, Zero grade) to 500 °C (in keeping with earlier studies, 450 °C was employed for the V_2O_5/SiO_2) and held for 6 h. The procedure for the aqueous preparations was the same as the nonaqueous preparations, except that the drying and initial calcination steps were performed in ambient air and under flowing air (Airgas, Zero grade), respectively. The surface modified SiO_2 supports, Al_2O_3/SiO_2, TiO_2/SiO_2, ZrO_2/SiO_2, were synthesized with 5 wt % metal oxide loadings on silica. The model catalysts, V_2O_5/SiO_2, CrO_3/SiO_2, MoO_3/SiO_2, WO_3/SiO_2, and Re_2O_7/SiO_2, were synthesized with 3 wt % metal oxides on silica (in keeping with earlier studies, 5 wt % was employed for V_2O_5/SiO_2), identified henceforth as MOx/SiO_2.

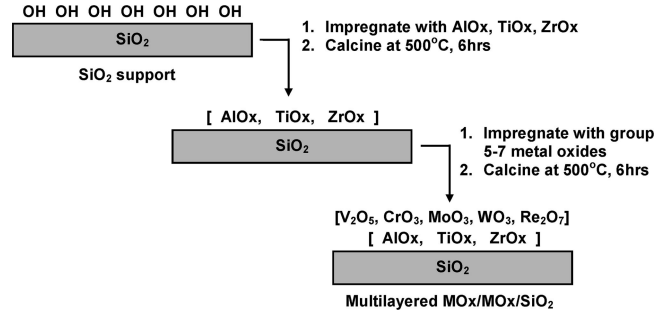

Figure 1. Schematic of the synthesis of multilayered supported metal oxide catalysts via incipient wetness impregnation. Step one, surface modification of the SiO_2 support with surface AlOx, TiOx, and ZrOx species. Step two, anchoring of the group 5−7 metal oxides on the surface modified SiO_2 support.

The multilayered catalysts were synthesized similarly to the model catalysts, however, the incipient wetness impregnation of the group 5−7 transition metal oxide overlayers were added to an existing calcined alumina-, titania-, and zirconia-surface modified SiO_2 support (depicted in Figure 1). The calcination procedures followed that of the model catalysts above for the corresponding systems. All metal oxides impregnated onto the surface modified SiO_2 supports were synthesized with 3 wt % (CrO_3, MoO_3, WO_3, and Re_2O_7, with exception to V_2O_5 at 5 wt % for the purposes of following earlier studies) and identified henceforth as $M_1Ox/M_2Ox/SiO_2$ (for example, $CrO_3/AlOx/SiO_2$).

2.2. In situ Raman Spectroscopy. The Raman spectra of the silica-supported metal oxide catalysts were obtained by a high resolution, dispersive Raman spectrometer system (Horiba-Jobin Yvon LabRam HR) equipped with three laser excitations (532, 442, and 325 nm), detailed elsewhere.[11] The sample power of the visible lasers at 532 (green) and 442 nm (violet) are 10 and 28 mW, respectively, and the sample of the UV laser at 325 nm (not visible) is ∼7 mW. The lasers were focused on the samples with a confocal microscope equipped with a 50X long working distance objective (Olympus BX-30-LWD) for the visible lasers and 15X objective (OFR LMU-15X-NUV) for the UV laser. Neither loss of signal intensity during the collection period or a "burn" spot from the laser beam onto the catalyst surface was observed to suggest any beam damage. In addition, laser-induced heating of the sample was negligible since the Raman spectra are collected at high temperatures above 450 °C. The LabRam HR spectrometer was optimized for the best spectral resolution by employing a 900 groves/mm grating (Horiba-Jobin Yvon 51093140HR) for the visible lasers and a 2400 grooves/mm grating (Horiba-Jobin Yvon 53011140HR) for the UV laser. The spectral resolution for both gratings is ∼2 cm^{-1}. The calibration of each laser line was independently measured by a Hg lamp for the zero position and linearity of the gratings. The wavenumber calibration of the Raman spectrograph was checked using the silicon line at 520.7 cm^{-1}. The Rayleigh scattered light was rejected with holographic notch filters (Kaiser Super Notch) with window cutoffs of ∼100 cm^{-1} for the visible lasers and ∼300 cm^{-1} for the UV laser. The Raman system was equipped with a UV-sensitive liquid-N_2 cooled CCD detector (Horiba-Jobin Yvon CCD-3000V).

The catalyst samples, typically consisting between 5−10 mg of loose powder, were placed in an environmentally controlled high temperature cell reactor (Linkam TS1500) containing a quartz window and O-ring seals that were cooled by flowing water. The sample temperature was controlled by a temperature

programmer (Linkam TMS94). The temperature calibration correction and in situ reactor cell capabilities are detailed elsewhere.[11] Typical reactor cell conditions were 450−700 °C, 10−30 °C/min heating and cooling rates, atmospheric pressure, and ∼30 sccm gas flowrates metered by mass flow controllers (Brooks, Model 5850E series). The protocol for obtaining in situ Raman spectra under the dehydrated oxidizing (O_2/Ar) environment is as follows. The samples were initially dehydrated in the in situ cell at 500 °C and held for 30 min under flowing 10% O_2/Ar (Airgas, certified, 10.00% O_2/Ar balance). Samples known to exhibit fluorescence were first pretreated in a separate programmable furnace (Thermolyne, Model 48000) at 500 °C for 2 h under ambient air. The Raman spectra were collected at 20 s/scan for 20 scans with a 200 μm size hole where only laser angles parallel to the incident beam were acquired from the light scattered by the catalyst sample. During the isotopic oxygen experiments, the Raman vibrations from the SiO_2 support (487, 606, and 800 cm^{-1}) were used as an internal standard for signal intensity.

Each dehydrated supported MOx/SiO_2 catalytic system is examined with combined in situ visible (532 and 442 nm) and UV (325 nm) Raman spectroscopy, and the Raman laser line that gave the clearest band distinction or best resolution is presented in this paper. The comparison of the effect of different laser excitation energies will be detailed in a subsequent paper. The use of multiple laser excitations avoids sample fluorescence that sometimes plagued earlier Raman measurements and also provides for the potential of resonance enhancement of weak Raman bands that may have been undetected in earlier studies.[17,49,50]

2.3. In situ UV−vis DRS Spectroscopy. The UV−vis DRS measurements were obtained with a Varian Cary 5E UV−vis−NIR spectrophotometer employing the integration sphere diffuse reflectance attachment (Harrick Praying Mantis Attachment, DRA-2), which was previously described.[11] The catalyst samples were loaded as loose powder (∼20 mg) into an in situ cell (Harrick, HVC-DR2) and the spectra were collected from 200−800 nm. The reflectance of the SiO_2 support was used as the baseline standard. For the supported M_1Ox/TiOx/SiO_2 systems, however, the strong titania absorbance was subtracted from the overall UV−vis DRS spectra by the corresponding supported 5% TiO_2/SiO_2. The catalyst temperature was accurately controlled by a temperature program controller (Harrick Scientific, Watlow Series 965 controller). The catalyst samples were calcined and dehydrated at 400 °C for 1 h under flowing 10% O_2/He (Airgas, certified, 9.735% O_2/He balance) at 30 sccm, then accumulated at 400 °C and also at room temperature after dehydration. The Kubelka−Munk function, $F(R_\infty)$, was extracted from the UV−vis DRS absorbance, and the edge energy (E_g) for allowed transitions was determined by finding the intercept of the straight line from the low-energy rise of the $[F(R_\infty)h\nu]^{1/n}$, where $n = 0.5$ for the direct allowed transition ion, versus $h\nu$, the incident photon energy.[51]

3. Results

3.1. Molecular Structure of Surface AlOx, TiOx, and ZrOx Species on SiO_2. The in situ Raman spectrum of the dehydrated SiO_2 support is shown in Figure 2 and contains three silica network bands at ∼1065, ∼800, and 410−450 cm^{-1} that have been assigned to the transverse-optical (TO) asymmetric stretch, Si−O−Si symmetrical stretching and network bending modes, respectively.[52−55] A weak band at 1200 cm^{-1} is also observed, typically assigned to the longitudinal-optical (LO) silica network, but will not be discussed in greater detail since it is just beyond the metal oxide vibrational region that is the focus of the study. The vibrational bands at 605 and 487 cm^{-1} have been assigned to the D2 and D1 defect modes attributed to tri- and tetra-cyclosiloxane rings, respectively,[53,56,57] and the 970 cm^{-1} Raman band arises from the Si-OH stretching mode of the surface hydroxyls.[54]

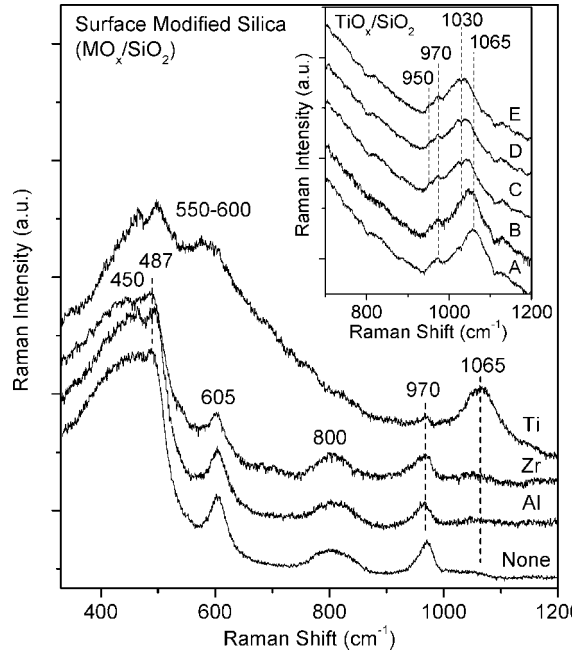

Figure 2. In situ Raman spectra of 5% AlOx-, ZrOx-, and TiOx-surface modified SiO_2 (5% MOx/SiO_2) using UV (325 nm) excitation under oxidizing conditions at 500 °C. The native dehydrated SiO_2 spectrum is provided as a reference. Raman spectrum of TiO_2/SiO_2 with 532 nm excitation has the equivalent vibrations, however, the Al_2O_3/SiO_2 and ZrO_2/SiO_2 spectra with 532 and 442 nm excitations are obscured by fluorescence. (Inset) Time-resolved in situ Raman spectra of dehydrated 5% TiO_2/SiO_2 (325 nm) at 500 °C during exposure to flowing $H_2{}^{18}O$ after approximately (A) 0, (B) 20, (C) 30, (D) 50, and (E) 80 min.

The in situ Raman spectra of surface modified SiO_2 supported catalysts (5% Al_2O_3/SiO_2, 5% TiO_2/SiO_2, and 5% ZrO_2/SiO_2) are presented in Figure 2. No significant spectral features can be observed upon the deposition of alumina and zirconia on the silica support except for perturbations of the 970 cm^{-1} band, which is most evident from TiOx/SiO_2. The decreased intensity the Si-OH band indicates consumption of the Si-OH hydroxyls by the deposited AlOx, TiOx, and ZrOx species and also confirmed by near-IR DRS at 7315 cm^{-1} (2ν).[19,20] The surface modification of the SiO_2 support by the deposited oxides leads to formation of bridging M−O−Si bonds and broadening of the 970 cm^{-1} band in the ZrO_2/SiO_2 Raman spectrum toward lower wavenumbers (∼940 cm^{-1}) related to the bridging Zr−O−Si linkages.[20] Therefore, the Al-, Zr-, and Ti-surface modifiers anchor to the silica at the Si−OH sites to create bridging M_2−O−Si bonds. Additional features are also present for the supported TiOx/SiO_2 sample. The TO mode of the silica network at 1065 cm^{-1} appears to be resonance Raman enhanced and the band at 550−600 cm^{-1} is possibly indicative of a small amount of polymeric Ti−O−Ti species. The band at 1065 cm^{-1}, upon exposure to oxygen-18 shown in Figure 2 (inset), shifts to ∼1030 cm^{-1} similar to earlier work by Galeener and Mikkelsen[54] on vitreous SiO_2 assigned to the silica network TO mode and, thus, cannot be assigned to other TiOx vibrations such as Ti=^{18}O, which would shift to ∼1015 cm^{-1} based on calculations from a simple diatomic oscillator.[10] The band at 970 cm^{-1} shifts to ∼950 cm^{-1}, indicative of surface exchanged

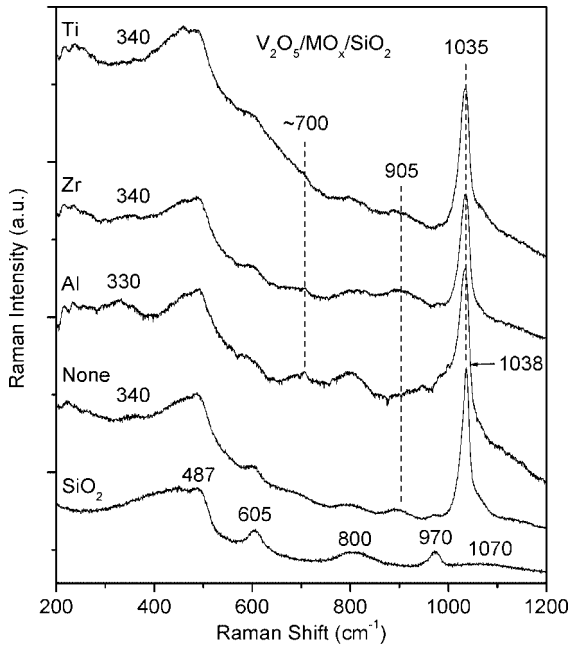

Figure 3. In situ Raman spectra (532 nm) of dehydrated supported 5% V_2O_5/SiO_2, 5% $V_2O_5/AlOx/SiO_2$, 5% $V_2O_5/ZrOx/SiO_2$, and 5% $V_2O_5/TiOx/SiO_2$ catalysts under oxidizing conditions at 600 °C. The native dehydrated SiO_2 spectrum is provided for reference. The corresponding spectra with 325 and 442 nm excitations exhibit weaker and broader surface vanadia species than the 532 nm spectra (not shown for brevity).

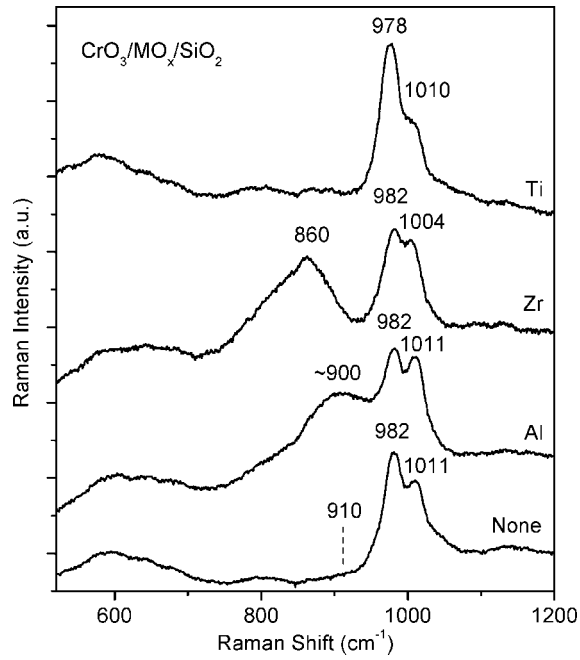

Figure 4. In situ Raman spectra (442 nm) of dehydrated supported 3% CrO_3/SiO_2, 3% $CrO_3/AlOx/SiO_2$, 3% $CrO_3/ZrOx/SiO_2$, and 3% $CrO_3/TiOx/SiO_2$ catalysts under oxidizing conditions at 500 °C. The spectra recorded with 325 nm excitation exhibited a dominant ~980 cm^{-1} band which overlapped with the ~1011 cm^{-1} band, and the spectra collected with 532 nm excitation revealed the same surface chromia band positions, but weaker vibrations due to fluorescence background signals (not shown for brevity).

oxygen of the Si−OH species.[10] Raman bands from crystalline TiO_2 and ZrO_2 nanoparticles (NPs) are not observed and are consistent with the presence of surface M_2Ox species on the silica support. The absence of Raman active bands for Al_2O_3 NPs does not allow for direct information about their presence with Raman spectroscopy.

In addition to in situ Raman spectroscopy, the surface modified SiO_2 supports have also been extensively characterized under dehydrated conditions with in situ IR, UV−vis DRS, XPS, XANES and solid-state ^{27}Al-NMR. However, only their dehydrated surface M_2Ox molecular structures will be summarized here.[19,20,46,58] The dehydrated supported 5% TiO_2/SiO_2 and 5% ZrO_2/SiO_2 catalysts consist of 100% dispersed surface TiOx and ZrOx species on the SiO_2 support and correspond to slightly less than half-monolayer coverage.[20,46] The dehydrated surface TiOx species are present as TiO_4 and TiO_5 coordinated species. The coordination environment of the surface ZrOx species under dehydrated conditions has not been determined. The dehydrated surface AlOx species on SiO_2 primarily contain AlO_4 coordination with a minor amount of surface AlO_5 species.[58] In summary, supported TiO_2/SiO_2 and supported ZrO_2/SiO_2 consists of $(OH)-M-(O-Si)_3$, while supported Al_2O_3/SiO_2 consists of $(O^-)-Al-(O-Si)_3$ where the extra proton (Brønsted acid site) is on the ligand oxygen under dehydrated conditions.

3.2. In Situ Raman Spectroscopy of Supported Group 5−7 Metal Oxides on Surface Modified SiO_2. ***3.2.1. Supported $V_2O_5/M_2Ox/SiO_2$.*** The in situ Raman spectra of the dehydrated model supported V_2O_5/SiO_2 catalyst and the promoted vanadia systems are shown in Figure 3. The model supported V_2O_5/SiO_2 catalyst system exhibits a sharp and intense vibration at 1038 cm^{-1} that has been assigned to the terminal symmetric V═O stretch (ν_s) of isolated surface VO_4 species.[46,59−63] The position of this vibration is consistent with the monoxo V═O structure present in the $H_3SiMo_{11}VO_{40}$ Keggin structure (1034 cm^{-1}) as well as with density functional theoretical (DFT) calculations (1038−1047 cm^{-1}).[64−66] In addition, weaker bands at 340 and 905 cm^{-1} are also present and are assigned to the bending O−V−O (δ) and bridging V−O−Si stretching modes. The weak shoulder band at 1070 cm^{-1} is characteristic of the TO mode of the silica network. The in situ Raman spectra of the dehydrated, supported $V_2O_5/AlOx/SiO_2$, $V_2O_5/TiOx/SiO_2$ and $V_2O_5/ZrOx/SiO_2$ catalysts give rise to a single main band at ~1035−1040 cm^{-1} assigned to the ν_s(V═O) stretching mode. The close proximity to the model system indicates that the species are similar, thereby, confirming the monoxo V═O species. A new band at ~700 cm^{-1} is tentatively assigned to the stretching mode of the corresponding V−O−Al/V−O−Zr/V−O−Ti bridging bonds and becomes more intense with increased vanadia and additive concentrations.[19−21,47] Sharp Raman bands from crystalline V_2O_5 NPs (994, 697, 284, and 144 cm^{-1}) are not present in any of the catalysts and all other Raman vibrations arise from the silica support.

3.2.2. Supported $CrO_3/M_2Ox/SiO_2$. The in situ Raman spectrum of dehydrated model supported CrO_3/SiO_2 catalyst is shown in Figure 4 and exhibits two main vibrations at 982 and 1011 cm^{-1} that have been assigned to the symmetric dioxo $Cr(=O)_2$ and monoxo Cr═O stretch modes, respectively.[11,15] The asymmetric $Cr(=O)_2$ stretch (ν_{as}) is not readily evident against the stronger monoxo Cr═O stretch, but is expected to vibrate at ~1010−1015 cm^{-1}. A very weak band at ~910 cm^{-1} is attributed to the bridging Cr−O−Si support bond. The absence of strong characteristic bands of crystalline Cr_2O_3 NPs at 545 and 603 cm^{-1} confirms that the chromia species are completely dispersed on the SiO_2 support. The in situ Raman spectra of the dehydrated supported $CrO_3/AlOx/SiO_2$, $CrO_3/ZrOx/SiO_2$, and $CrO_3/TiOx/SiO_2$ catalysts under oxidizing conditions are also shown in Figure 4. Although the surface dioxo $Cr(=O)_2$ (978−982 cm^{-1}) and monoxo Cr═O (1004−1011 cm^{-1}) species are also present for the multilayered catalysts,

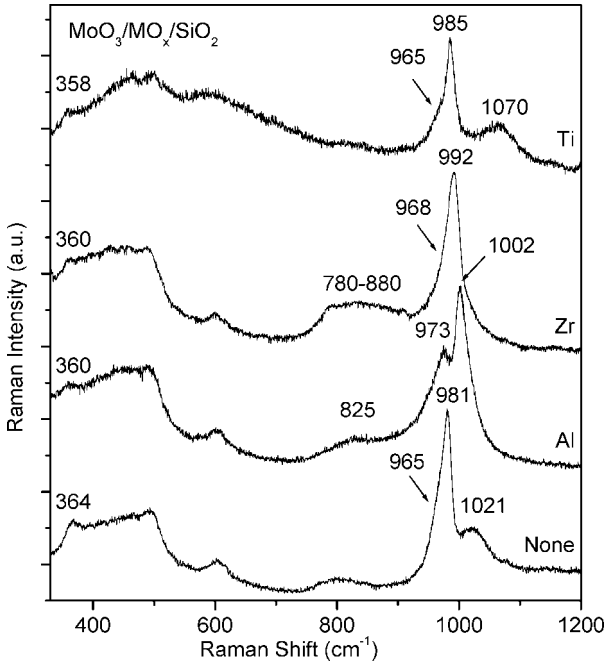

Figure 5. In situ Raman spectra (325 nm) of dehydrated supported 3% MoO_3/SiO_2, 3% $MoO_3/AlOx/SiO2$, 3% $MoO_3/ZrOx/SiO_2$, and 3% $MoO_3/TiOx/SiO_2$ under oxidizing conditions at 500 °C. The spectra collected with 442 and 532 nm excitation exhibited the equivalent vibrations, except for the 3% $MoO_3/AlOx/SiO_2$ (532 nm), which was obscured by fluorescence (not shown for brevity).

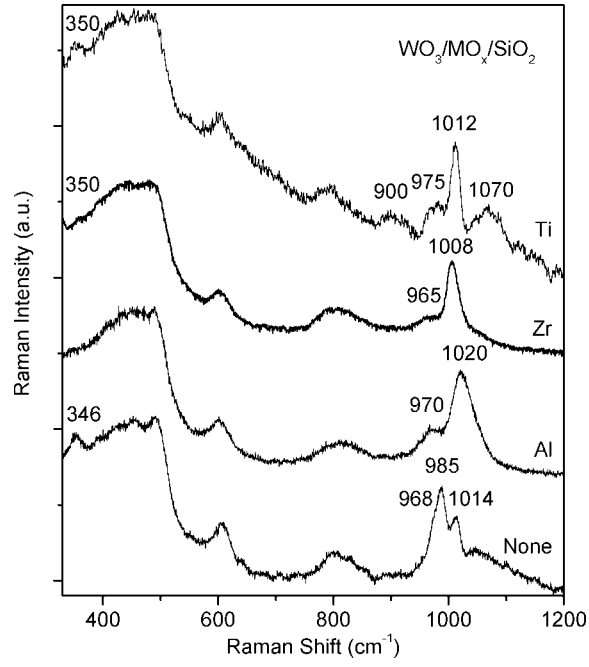

Figure 6. In situ Raman spectra of dehydrated supported 3% WO_3/SiO_2, 3% $WO_3/AlOx/SiO_2$, 3% $WO_3/ZrOx/SiO_2$, and 3% $WO_3/TiOx/SiO_2$ under oxidizing conditions at 600 °C. 3% WO_3/SiO_2 and 3% $WO_3/TiOx/SiO_2$ catalysts were collected with 532 nm excitation and 3% $WO_3/AlOx/SiO_2$ and 3% $WO_3/ZrOx/SiO_2$ were collected with 325 nm excitation. Not shown for brevity are the spectra of 3% $WO_3/ZrOx/SiO_2$ (532 nm), which exhibited weak signals; 3% $WO_3/AlOx/SiO_2$ (442 and 532 nm), which were obscured by fluorescence; and 3% WO_3/SiO_2 and 3% $WO_3/TiOx/SiO_2$ (325 nm excitation), which exhibited a strong resonance enhancement of the ~1065 cm^{-1} band assigned to the TO mode of the silica network.

their intensity ratio varies with the presence of the AlOx, TiOx, or ZrOx additives. The ratio of dioxo to monoxo surface chromia species are roughly ~2:1 for the model CrO_3/SiO_2 and $CrO_3/TiOx/SiO_2$ catalysts and ~1:1 for the supported $CrO_3/AlOx/SiO_2$ and $CrO_3/ZrOx/SiO_2$ catalysts from deconvolution of the Raman spectra. In addition, a strong and broad band is present which is centered at ~860−900 cm^{-1} for the supported $CrO_3/AlOx/SiO_2$ and $CrO_3/ZrOx/SiO_2$ catalysts that is assigned to the bridging Cr−O−Al and Cr−O−Zr vibrations, respectively.[67−69] The Raman bands from crystalline Cr_2O_3 NPs (545 and 603 cm^{-1}) are not present in any of the supported CrO_3 catalyst samples; all other Raman vibrations arise from the silica support.

3.2.3. Supported $MoO_3/M_2Ox/SiO_2$. The in situ Raman spectrum of the dehydrated supported MoO_3/SiO_2 model catalyst is shown in Figure 5 and consists of a main band at 981 cm^{-1} (dioxo $\upsilon_s(Mo(=O)_2)$ stretch), a shoulder at 965−975 cm^{-1} (dioxo $\upsilon_{as}(Mo(=O)_2)$ stretch), and a weak vibration at 364 cm^{-1} (δ(O−Mo−O) mode).[10,11,70−75] In addition, the weak band at 1021 cm^{-1} has been previously assigned to surface monoxo Mo=O species.[10,11] The absence of the sharp crystalline MoO_3 NPs band at 820 cm^{-1} is consistent with the presence of only dispersed surface MoOx species on the SiO_2 support. The in situ Raman spectra of the supported $MoO_3/AlOx/SiO_2$, $MoO_3/ZrOx/SiO_2$, and $MoO_3/TiOx/SiO_2$ catalysts under oxidizing conditions are also presented in Figure 5. All the surface modified SiO_2 catalysts do not contain the Raman band of the surface monoxo Mo=O species at ~1020 cm^{-1}. The supported $MoO_3/TiOx/SiO_2$ and $MoO_3/ZrOx/SiO_2$ catalysts give rise to Raman bands at 985 and 992 cm^{-1}, respectively, assigned to surface dioxo $Mo(=O)_2$ species.[76] The shift from 981 to 985−992 cm^{-1} reflect distortions of the dioxo surface $Mo(=O)_2$ species caused by interaction with the surface ZrOx and TiOx additives of the surface modified SiO_2 support. The corresponding asymmetric surface dioxo $Mo(=O)_2$ stretch occurs as a weak shoulder at ~965−968 cm^{-1} on the strong symmetric stretch. The somewhat higher wavenumber value of 1002 cm^{-1} for the supported $MoO_3/AlOx/SiO_2$ system may reflect the presence of some monooxo surface MoO_5 species. The corresponding band at ~973 cm^{-1} for the supported $MoO_3/AlOx/SiO_2$ catalyst is most likely from surface hydroxyl groups present on this catalyst as well as the possible presence of some surface dioxo species. The weak band at ~360 cm^{-1} is assigned to the δ(O−Mo−O) mode. The weak and broad bands at ~825−880 cm^{-1} observed for supported $MoO_3/AlOx/SiO_2$ and $MoO_3/ZrOx/SiO_2$ catalysts are assigned to bridging M−O−Al and Mo−O−Zr bonds, respectively.[3,74,77] The characteristic Raman band of crystalline MoO_3 NPs (~820 cm^{-1}) is not present and all other Raman vibrations arise from the silica support.

3.2.4. Supported $WO_3/M_2Ox/SiO_2$. The in situ Raman spectrum of dehydrated model supported WO_3/SiO_2 catalyst is shown in Figure 6 and possesses two major bands at 985 and 1014 cm^{-1} assigned to the dioxo $\upsilon_s(W(=O)_2)$ and monoxo $\upsilon_s(W=O)$ stretching modes, respectively. The $\upsilon_{as}(W(=O)_2)$ vibration appears as a weak shoulder at 968 cm^{-1} and the δ(O−W−O) mode occurs at 346 cm^{-1}.[11,78] The absence of crystalline WO_3 NPs, which gives rise to strong Raman bands at 805 and 712 cm^{-1}, indicates that the supported tungsten oxide species are completely dispersed on the SiO_2 support. The in situ Raman spectra of the dehydrated supported $WO_3/AlOx/SiO_2$, $WO_3/ZrOx/SiO_2$, and $WO_3/TiOx/SiO_2$ catalysts are also presented in Figure 6. The molecular structure of the surface WOx species is altered by interaction with the surface modified SiO_2 support. The major Raman band of the surface WOx species is found at ~1008−1020 cm^{-1} that is characteristic of surface monoxo W=O species. A weak band exists at 965−975 cm^{-1} arising from a combination of a trace amount of dioxo surface $W(=O)_2$

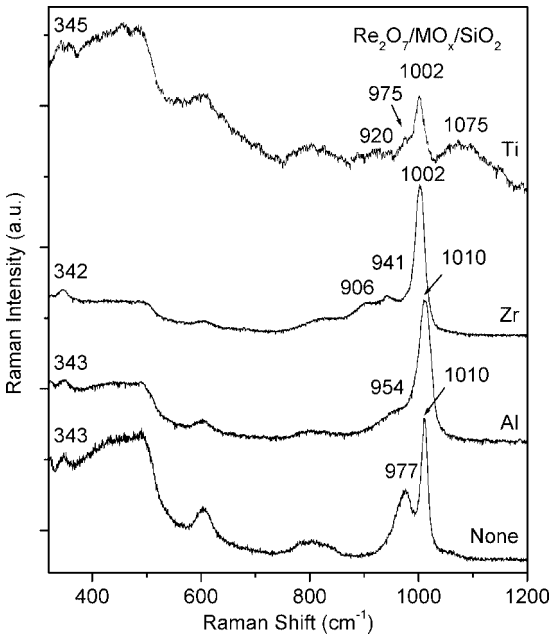

Figure 7. In situ Raman spectra (325 nm) of dehydrated supported 3% Re_2O_7/SiO_2, 3% $Re_2O_7/AlOx/SiO_2$, 3% $Re_2O_7/ZrOx/SiO_2$, and 3% $Re_2O_7/TiOx/SiO_2$ (532 nm for 3% $Re_2O_7/TiOx/SiO_2$ only) under oxidizing conditions at 450 °C. The corresponding 532 nm excitation spectra exhibited the equivalent vibrations, but weaker overall signal intensities (not shown for brevity).

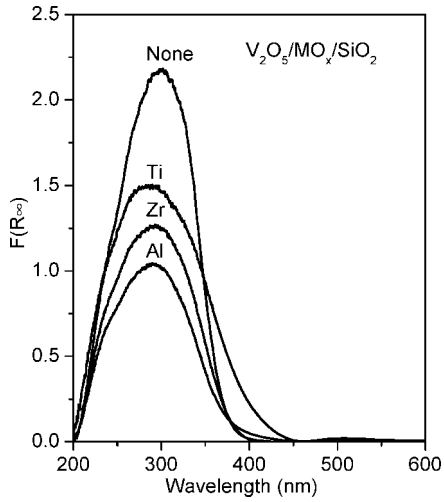

Figure 8. In situ UV−vis DRS spectra of dehydrated supported 5% V_2O_5/SiO_2, 5% $V_2O_5/AlOx/SiO_2$, 5% $V_2O_5/ZrOx/SiO_2$, and 5% $V_2O_5/TiOx/SiO_2$ (with subtracted 5% TiO_2/SiO_2) under oxidizing conditions at 400 °C.

species and exposed Si−OH sites. The monoxo/dioxo ratios ($A_{\sim1020\ cm^{-1}}/A_{\sim970\ cm^{-1}}$) for the supported tungsten oxide catalysts are 0.6, 4.0, 2.7, 1.8 supported WO_3/SiO_2, $WO_3/AlOx/SiO_2$, $WO_3/ZrOx/SiO_2$, and $WO_3/TiOx/SiO_2$, respectively. Only the supported $WO_3/TiOx/SiO_2$ catalyst possesses a Raman band at ~900 cm^{-1} that is indicative of bridging W−O−Ti bonds. This assignment is made by similarity to the supported vanadia and molybdena systems where the V−O−support and Mo−O−support vibrations give rise to bands at 905 and ~928 cm^{-1}, respectively, based on isotopic oxygen labeling and DFT calculations.[10,65,66,76] The weak band at ~350 cm^{-1} is characteristic of the δ(O−W−O) mode of the surface WOx species. The characteristic Raman bands of crystalline WO_3 NPs are not present and all other Raman vibrations are those from the silica support.

3.2.5. Supported $Re_2O_7/M_2Ox/SiO_2$. The in situ Raman spectrum of the dehydrated supported Re_2O_7/SiO_2 model catalyst is shown in Figure 7 and exhibits two main surface ReOx vibrations: a sharp band at 1010 cm^{-1} (symmetric stretching mode of trioxo Re(=O)$_3$ species) and a broad band at 977 cm^{-1} (overlapping asymmetric Re(=O)$_3$ stretch and Si−OH hydroxyls vibration).[10,11,79,80] The weak Raman band at 343 cm^{-1} is the corresponding bending O−Re−O mode. Crystalline Re_2O_7 (major Raman bands at 993, 854, 831, and 798 cm^{-1}) is not present for supported Re_2O_7 catalysts since the surface rhenium oxide species readily recombine to form volatile gaseous Re_2O_7 dimers that precludes formation of Re_2O_7 crystallites.[9,79,81,82] The in situ Raman spectra of dehydrated supported $Re_2O_7/AlOx/SiO_2$, $Re_2O_7/ZrOx/SiO_2$, and $Re_2O_7/TiOx/SiO_2$ catalysts are presented in Figure 7 and give rise to a strong band at ~1002−1010 cm^{-1} characteristic of the trioxo υ_s(Re(=O)$_3$) functionality. The similar band positions for the unpromoted and promoted supported rhenia catalysts reveal that the surface oxide additives do not significantly alter the structure of the surface ReOx species. The corresponding asymmetric stretch appears between 941−975 cm^{-1} for the surface modified SiO_2 catalysts and the δ(O−Re−O) mode is also present at 342−345 cm^{-1}. The bridging Re−O−Ti and Re−O−Zr vibrations are present at ~905−920 cm^{-1}. The Raman vibrations at 450−487, 605, and 800 cm^{-1} are from the silica support.

3.3. In Situ UV−vis Diffuse Reflectance Spectroscopy (DRS). ***3.3.1. Supported $V_2O_5/M_2Ox/SiO_2$.*** The in situ UV−vis DRS spectrum of the model supported V_2O_5/SiO_2 catalyst under dehydrated oxidizing conditions, shown in Figure 8, consist of a single ligand-to-metal charge transfer (LMCT) transition at 290 nm. The corresponding edge energy (Eg) value of 3.5 eV, listed in Table 1, is assigned to isolated VO_4 surface species by comparison with VOx reference compounds.[47] The in situ UV−vis DRS spectra of $V_2O_5/AlOx/SiO_2$, $V_2O_5/TiOx/SiO_2$ and $V_2O_5/ZrOx/SiO_2$, also presented in Figure 8, give rise to a single LMCT band maxima at ~283−288 nm with corresponding Eg values of 3.4−3.6 eV.[19−21,47] The UV−vis spectroscopic results reveal that the surface vanadium oxide species of the promoted vanadia systems predominantly exist as isolated surface VO_4 species on the SiO_2 support since the LMCT band maxima and the Eg values remain reasonably constant for the model and promoted catalysts.

3.3.2. Supported $CrO_3/M_2Ox/SiO_2$. The in situ UV−vis DRS of the dehydrated model supported CrO_3/SiO_2 catalyst under oxidizing conditions has been shown to exhibit multiple LMCT transitions at ~250, ~340, and ~460 nm where the band maxima do not shift with surface coverage. From the best linear fit in the lower absorption region, the calculated Eg value is ~2.4 eV, which is consistent with isolated surface chromia species. The UV−vis DRS band maxima for the dehydrated supported CrO_3/SiO_2 catalysts are also in good agreement with highly dispersed, isolated Cr(VI) species in a silica xerogel monolith.[15] The in situ UV−vis DRS of dehydrated supported $CrO_3/AlOx/SiO_2$, $CrO_3/ZrOx/SiO_2$, and $CrO_3/TiOx/SiO_2$ catalyst samples are presented in Figure 9 (left). The promoted supported chromia catalysts also exhibit multiple LMCT transitions at ~250−270 and 350−360 nm, however, a third transition is absent. Previous reports for dehydrated supported $CrO_3/SiO_2-Al_2O_3$ confirm that the third transition at ~450 nm only exists at higher Si:Al ratio,[83,84] which is similar for the present supported CrO_3/SiO_2 catalyst under dehydrated conditions. Therefore, it is suggested that the third transition at ~450 nm arises from the LMCT of the O (2p) to Cr (d) orbitals of the surface CrOx species on silica. The absence of this band in the presence of surface AlOx species is indicative of structural

TABLE 1: Table of LMCT Band Maxima and Eg Values under Dehydrated, Oxidizing Conditions for the Model MOx/SiO_2 Systems and the Surface Modified SiO_2 Catalyst Systems

catalyst	MOx/SiO_2		V_2O_5/MOx/SiO_2		CrO_3/MOx/SiO_2	
MOx	bands (nm)	Eg (eV)	bands (nm)	Eg (eV)	bands (nm)	Eg (eV)
none			290	3.5[11]	246, 337, 460	2.4[11]
Al_2O_3			288	3.6	250, 350	4.0
ZrO_2	204	5.7[20]	288	3.5	250, 350	4.0
TiO_2	248	4.2[21]	283	3.4	270, 360	4.8
catalyst	MoO_3/MOx/SiO_2		WO_3/MOx/SiO_2		Re_2O_7/MOx/SiO_2	
MOx	bands (nm)	Eg (eV)	band (nm)	Eg (eV)	bands (nm)	Eg (eV)
none	237, 274	4.1[11]	231, 265	4.1[11]	240	4.7[11]
Al_2O_3	217	4.9	224	5.0	232	4.8
ZrO_2	235	4.8	227	5.2	238	4.7
TiO_2	226	4.5	232	4.6		

changes associated with the surface CrOx species. In agreement with the Raman spectral results, crystalline Cr_2O_3 NPs are not present (d−d transition at ∼600−700 nm) and reflect the presence of only fully dispersed surface chromia species on the surface modified SiO_2. The corresponding Eg values are ∼4−4.8 eV and are listed in Table 1. The higher Eg values correspond to the change in the electronic structures of the surface CrOx species perturbed by the support modifiers (ligands). The high Eg values reflect the isolated nature of the surface CrOx species in the dehydrated supported CrO_3/AlOx/SiO_2, CrO_3/ZrOx/SiO_2, and CrO_3/TiOx/SiO_2 catalysts.

3.3.3. Supported MoO_3/M_2Ox/SiO_2. The in situ UV−vis DRS spectrum of the dehydrated supported MoO_3/SiO_2 model catalysts possesses two LMCT transitions with band maxima at ∼237 and 274 nm (shown by deconvolution with gray dash lines in Figure 9 (right)). The corresponding UV−vis DRS Eg value from the rise of the lower absorption in the low-energy region is 4.1 eV. Comparison of the Eg value for the dehydrated supported MoO_3/SiO_2 catalysts with known MoOx molecular structures, for example $Al_2(MoO_4)_3$ and $MgMoO_4$,[11,81,85] reveals that the molybdena species is consistent with isolated monomeric MoOx structure. In situ UV−vis DRS spectra of multilayered, dehydrated MoO_3/AlOx/SiO_2, MoO_3/ZrOx/SiO_2, and MoO_3/TiOx/SiO_2 under oxidizing conditions are also presented in Figure 9 (right). Crystalline MoO_3 NPs are not detected, expected to arise at ∼400 nm, and indicate that the supported molybdena species on the promoted catalysts are fully dispersed. Unlike the model supported MoO_3/SiO_2 system, the supported MoO_3/AlOx/SiO_2, MoO_3/ZrOx/SiO_2, and MoO_3/TiOx/SiO_2 catalysts gives rise to only a single LMCT transition at ∼217−235 nm with corresponding Eg values of 4.5−4.9 eV (see Table 1). Similar to the supported chromia system where the modifiers eliminate the higher LMCT transition, the second transition at ∼275 nm for supported MoO_3/SiO_2 is associated with the LMCT of the O (2p) to Mo (d) orbitals of the surface MoOx on silica. The absence of this band for the supported MoO_3/MO_x/SiO_2 catalyst reflects the change of the surface MoOx species. The lower LMCT band maximum and corresponding higher Eg value indicates a strong electronic change in the LMCT between the surface modifiers and the molybdena species. The higher Eg values reflect a more localized electronic structure compared to the model system and confirm that the dehydrated supported MoO_3/AlOx/SiO_2, MoO_3/ZrOx/SiO_2, and MoO_3/TiOx/SiO_2 catalyst samples consist of isolated monomeric MoOx species.

3.3.4. Supported WO_3/M_2Ox/SiO_2. The in situ UV−vis DRS of the dehydrated model supported WO_3/SiO_2 catalyst exhibit

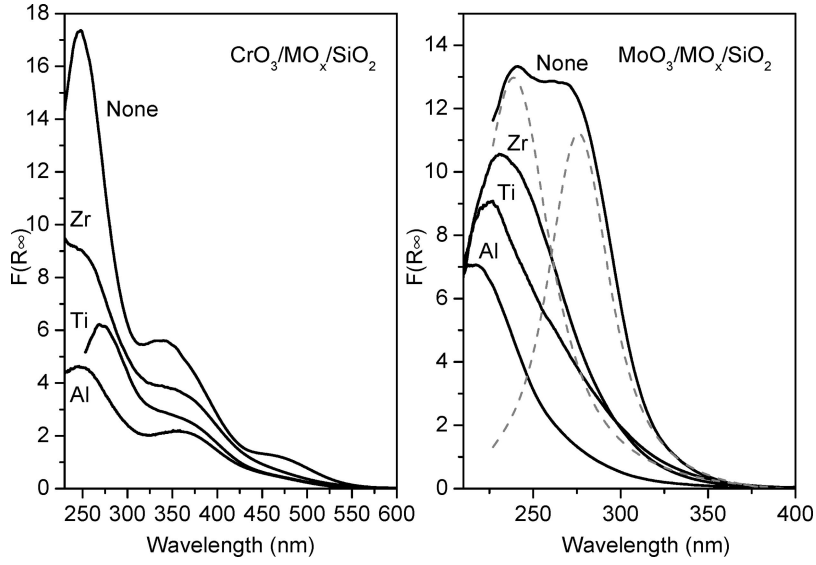

Figure 9. In situ UV−vis DRS spectra of dehydrated (left) supported 3% CrO_3/SiO_2, 3% CrO_3/AlOx/SiO_2, 3% CrO_3/ZrOx/SiO_2, and 3% CrO_3/TiOx/SiO_2 (with subtracted 5% TiOx/SiO_2), and (right) supported 3% MoO_3/SiO_2, 3% MoO_3/AlOx/SiO_2, 3% MoO_3/ZrOx/SiO_2, and 3% MoO_3/TiOx/SiO_2 (with subtracted 5% TiOx/SiO_2) under oxidizing conditions at 400 °C. Gray dash lines represent deconvolution bands for the supported 3% MoO_3/SiO_2 spectrum only.

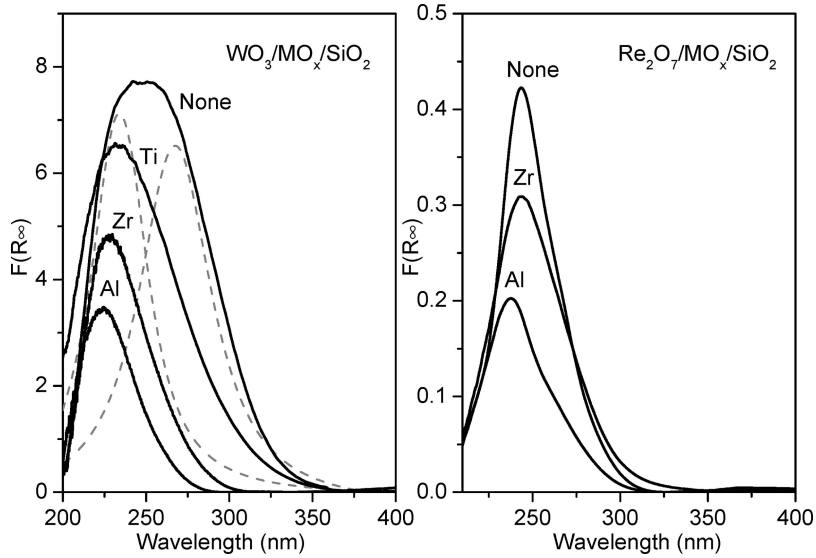

Figure 10. In situ UV−vis DRS spectra of dehydrated (left) supported 3% WO_3/SiO_2, 3% $WO_3/AlOx/SiO_2$, 3% $WO_3/ZrOx/SiO_2$, and 3% $WO_3/TiOx/SiO_2$ (with subtracted 5% $TiOx/SiO_2$), and (right) supported 3% Re_2O_7/SiO_2, 3% $Re_2O_7/AlOx/SiO_2$, and 3% $Re_2O_7/ZrOx/SiO_2$ (not shown is 3% $Re_2O_7/TiOx/SiO_2$) under oxidizing conditions at 400 °C. Gray dash lines represent deconvolution bands for the supported 3% WO_3/SiO_2 spectra.

band maxima at ~231 and 265 nm (shown by deconvolution with gray dash lines in Figure 10 (left)), similarly with MoO_3/SiO_2 model catalyst. The corresponding Eg value is 4.1 eV. Comparison with the Eg values of known isolated WO_4 compounds, for example ZrW_2O_8 and $Al_2(WO_4)_3$,[11,86,87] reveals that dehydrated tungsta species are predominantly isolated surface WOx species. In situ UV−vis DRS spectra of multilayered dehydrated supported $WO_3/AlOx/SiO_2$, $WO_3/ZrOx/SiO_2$, and $WO_3/TiOx/SiO_2$ catalyst samples under oxidizing conditions are shown in Figure 10 (left). The promoted catalysts do not contain crystalline WO_3 NPs which would give rise to a transition at ~400 nm. Similar to the promoted molybdena system, the supported $WO_3/AlOx/SiO_2$, $WO_3/ZrOx/SiO_2$, and $WO_3/TiOx/SiO_2$ catalysts gives rise to only a single LMCT transition at 224−232 nm, with corresponding Eg values at 4.6−5.2 eV (see Table 1). The narrow LMCT band and corresponding higher Eg values of the promoted catalysts indicate that the tungsta species are different than the model supported WO_3/SiO_2 catalyst system and consist of a different structure. The higher Eg values likely correspond to the structural differences of the surface tungsta species observed from the Raman results. Nevertheless, the higher Eg values of the supported $WO_3/AlOx/SiO_2$, $WO_3/ZrOx/SiO_2$, and $WO_3/TiOx/SiO_2$ catalysts reflect the isolated nature of the dehydrated surface WOx species.

3.3.5. Supported $Re_2O_7/M_2Ox/SiO_2$. The in situ UV−vis DRS of the dehydrated supported Re_2O_7/SiO_2 model catalysts give rise to a single LMCT transition at 240 nm with a corresponding Eg value of 4.7 eV. The UV−vis DRS band maxima and Eg values for the dehydrated supported Re_2O_7/SiO_2 catalysts are comparable to the rhenia reference compounds with isolated ReOx molecular structures.[11] In situ UV−vis DRS spectra of dehydrated supported $Re_2O_7/AlOx/SiO_2$ and $Re_2O_7/ZrOx/SiO_2$ catalysts, under oxidizing conditions are presented in Figure 10 (right). The promoted rhenia catalysts give rise to a single LMCT transition at ~232−238 nm with corresponding Eg values of 4.7−4.8 eV (see Table 1). The strong absorbance of the $TiOx/SiO_2$ overwhelms the spectrum of rhenia contribution from supported $Re_2O_7/TiOx/SiO_2$ and the spectrum, thus, is not shown but is expected to follow $Re_2O_7/AlOx/SiO_2$ and $Re_2O_7/ZrOx/SiO_2$. The similar band maxima and Eg value to the model and promoted catalysts indicates that all the rhenia consist of similar surface structures. Therefore, the dehydrated surface rhenia species on the promoted silica supports consist of isolated ReOx structures.

4. Discussion

The in situ UV−vis and Raman bands and their assignments for the dehydrated surface M_2Ox (M_2 = Al, Zr and Ti) and M_1Ox (M_1 = V, Cr, Mo, W and Re) species on native SiO_2 and surface modified SiO_2 catalyst samples are summarized in Table 2, respectively. The relatively high UV−vis Eg values reflect the isolated nature of the dehydrated surface MOx species on the native SiO_2 and surface modified silica supports. Some of the structural issues surrounding each of the SiO_2-supported metal oxide systems are further elaborated upon below.

4.1. Anchoring Sites for Surface M_1Ox on Surface Modified SiO_2. Insights about the anchoring sites for the dehydrated surface M_1Ox species (VOx, CrOx, MoOx, WOx, and ReOx) on the M_2Ox surface modified SiO_2 primarily come from the Raman spectra. The Raman spectra demonstrate that the molecular structures of the surface M_1Ox species are altered by the presence of the surface M_2Ox species on silica. For supported VOx and ReOx, the presence of surface M_1Ox results in minor shifts of the metal oxo Raman bands and in the relative intensity of the Raman bands for surface ReOx. For the supported group 6 metal oxides, the presence of the surface M_2Ox affects the monoxo/dioxo ratio of the surface M_1Ox species. For example, the supported WO_3/SiO_2 gives rise to a dominant Raman band at 985 cm^{-1} (dioxo $\upsilon_s(W(=O)_2)$) and a minor Raman band at 1014 cm^{-1} (monoxo $\upsilon_s(W=O)$) that transform to monoxo $\upsilon_s(W=O)$ species with a Raman band at 1020 cm^{-1} for the supported $WO_3/Al_2O_3/SiO_2$ catalyst system. Furthermore, the monoxo $\upsilon_s(W=O)$ Raman band position at 1020 cm^{-1} matches that for monoxo $\upsilon_s(W=O)$ species present in the supported WO_3/Al_2O_3 catalysts,[88] which reflects the preferential anchoring of the surface WOx species at the surface AlOx sites over exposed SiO_2 sites on the surface modified SiO_2 support. The preferential anchoring of the surface M_1Ox species on the M_2Ox species is a general phenomenon for anchoring of the group 5−7 transition metal oxides on the surface modified SiO_2 support.

TABLE 2: Raman Band Positions (cm^{-1}) of Dehydrated Surface Metal Oxide Species on Model Silica and Surface Modified SiO_2 Systems with Their Assignments

		$M_1Ox/M_2Ox/SiO_2$, M_1Ox =				
M_2O_x	assignments	V_2O_5	CrO_3	MoO_3	WO_3	Re_2O_7
none	ν(M═O)	1038 (s)	1011 (m)	1021 (m)	1014 (m)	
	ν_s(M(═O)$_2$)		982 (s)	981 (s)	985 (s)	
	ν_{as}(M(═O)$_2$)		[a]	965 (m)	968 (w)	
	ν_s(M(═O)$_3$)					1010 (s)
	ν_{as}(M(═O)$_3$)					977 (m)
	ν_s(M−O−S)	905 (w)	910 (vw)	[a]	900 (vw)	[a]
	δ(O−M−O)	340 (w)	[a]	364 (w)	346 (w)	343 (w)
Al_2O_3	ν(M═O)	1037 (s)	1011 (s)		1020 (s)	
	ν_s(M(═O)$_2$)		982 (s)	1002 (s)	970 (m)	
	ν_{as}(M(═O)$_2$)		[a]	973 (m)	[a]	
	ν_s(M(═O)$_3$)					1010 (s)
	ν_{as}(M(═O)$_3$)					954 (w)
	ν_s(M−O−S)	700[b], 925 (w)	900[b] (m)	825[b] (w)	[a]	[a]
	δ(O−M−O)	[a]	[a]	360 (w)	[a]	343 (w)
ZrO_2	ν(M═O)	1040 (s)	1004 (s)		1008 (s)	
	ν_s(M(═O)$_2$)		982 (s)	992 (s)	965 (m)	
	ν_{as}(M(═O)$_2$)		[a]	968 (w)	[a]	
	ν_s(M(═O)$_3$)					1002 (s)
	ν_{as}(M(═O)$_3$)					941 (w)
	ν_s(M−O−S)	700[b], 925 (w)	860[b] (m)	780−880[b] (m)	[a]	906[b] (w)
	δ(O−M−O)	[a]	[a]	360 (w)	350 (w)	342 (w)
TiO_2	ν(M═O)	1035 (s)	1010 (m)		1012 (s)	
	ν_s(M(═O)$_2$)		978 (s)	985 (s)	975 (w)	
	ν_{as}(M(═O)$_2$)		[a]	965 (w)	[a]	
	ν_s(M(═O)$_3$)					1002 (s)
	ν_{as}(M(═O)$_3$)					975 (w)
	ν_s(M−O−S)	700[b], 916 (w)	[a]	[a]	900[b] (w)	920[b] (w)
	δ(O−M−O)	340 (w)	[a]	358 (w)	350 (w)	345 (w)

[a] Vibration is too weak to be observed. [b] Tentatively assigned to bridging M−O−Al/M−O−Zr/M−O−Ti bonds.

The self-assembly of the surface M_1Ox species at the surface M_2Ox sites is most likely related to the acidic/basic nature of the surface −OH groups since anchoring of acidic surface M_1Ox initially occurs at the most basic surface −OH groups, followed by the neutral surface −OH groups and finally the most acidic surface −OH groups.[89] The acidity of the surface −OH groups is related to the electronegativity of the oxide support cation and increases with the support cation electronegativity (Zr ≈ Ti < Al < Si).[90] Consequently, the acidic surface M_1Ox species preferentially anchor at the more basic surface Zr−OH, Ti−OH, and Al−OH sites over the more acidic surface Si−OH sites.[19]

4.2. Molecular Structure of Multilayered Supported $M_1Ox/M_2Ox/SiO_2$ Catalysts. ***4.2.1. Supported $V_2O_5/M_2Ox/SiO_2$.*** The supported model V_2O_5/SiO_2 and multilayered $V_2O_5/M_2Ox/SiO_2$ catalyst systems give rise to main vanadia bands at 1038 and ∼1035−1040 cm^{-1}, respectively, that are assigned to the νs(V═O).[19−21,47] These values agree well with non-SiO_2 supported vanadia catalysts (V_2O_5/TiO_2, V_2O_5/ZrO_2 and V_2O_5/Al_2O_3) containing monoxo surface species, where ν_s(V═O) vibrates at ∼1025−1035 cm^{-1}.[91] The constancy of the V═O vibration indicates that the monoxo surface structure is maintained even with the addition of the surface modifiers. Furthermore, there is not an apparent ligand effect of the surface M_2Ox modifiers on the molecular structure of the surface vanadia species.

4.2.2. Supported $CrO_3/M_2Ox/SiO_2$. The in situ Raman spectra of multilayered supported $CrO_3/AlOx/SiO_2$, $CrO_3/ZrOx/SiO_2$, and $CrO_3/TiOx/SiO_2$ catalyst samples exhibit both dioxo ν_s(Cr(═O)$_2$) and monoxo ν_s(Cr═O) surface species (∼982 and ∼1004−1011 cm^{-1}, respectively) with the ratio of monoxo/dioxo species dependent on the presence of the surface M_2Ox species. The vibration of the monoxo Cr═O species agree well with the molecular structure of chromia supported on non-SiO_2 supports (Al_2O_3, TiO_2, and ZrO_2), which have also been proposed as monoxo CrOx structures, and contain three main CrOx bands: isolated monoxo Cr═O species (1005−1030 cm^{-1}), polymeric monoxo Cr═O (990−1010 cm^{-1}), and bridging Cr−O−Cr vibrations at 800−880 cm^{-1}.[68,69,92] For the multilayered chromia catalysts, previous findings for 1−3% CrO_3/3%TiO_2/SiO_2 also indicated a strong band at ∼980−984 cm^{-1} that was assigned to the terminal Cr═O of highly distorted tetrahedral monochromate species.[41] Unfortunately, this study utilized visible Raman excitation at 514.5 nm that encountered strong sample fluorescence and, furthermore, the researchers overlooked the shoulder at higher wavenumber (∼1000−1010 cm^{-1}), which likely arises from the monoxo Cr═O species. In the same study, it is interesting to see that 1% CrO_3/3%SiO_2/TiO_2 gave rise to bands at 1000, 982, and 830 cm^{-1}, where the 1000 and 982 cm^{-1} were found to be in the same intensity ratio. The researchers assigned the 1000 and 830 cm^{-1} bands to the polymeric surface CrOx on TiO_2 and the band at 982 cm^{-1} was ascribed to the monochromate CrOx on the SiOx phase. Based on the conclusions of the current study, however, it is likely that 1000 cm^{-1} arises from the monoxo Cr═O by interaction with a greater amount of available TiOx sites, the 982 cm^{-1} arises form the dioxo Cr(═O)$_2$ species on the SiOx additive overlayer, and the broad 830 cm^{-1} band is attributed to the bridging Cr−O−support. Additionally, previous reports of a similar supported $CrOx/SiO_2-Al_2O_3$ material using a 476.5 nm excitation reported a weak and broad band at 989 cm^{-1}, however, the spectra were limited against a fluoresced background and were subjected to a baseline subtraction which may have eliminated the presence of a second CrOx species.[15] In the present study conducted with Raman excitation at 442 nm excitation, the near equal chromium dioxo and monoxo Raman intensities for the supported $CrO_3/AlOx/SiO_2$ and $CrO_3/ZrOx/$

SiO_2 systems suggests that there is likely a 50% increase of monoxo species at the expense of the dioxo species compared to the model system. Therefore, the ratio of monoxo/dioxo surface MOx species on SiO_2 can be tuned by the addition of surface AlOx, TiOx, and ZrOx ligands, which suggests a strong effect of the interfacial interaction between the surface modifiers and surface chromia species. The chromia species on the surface modified silica exist as isolated, dioxo $(O{=})_2Cr(-O)_2$ species and isolated, monoxo $O{=}Cr(-O)_4$ species.

4.2.3. Supported $MoO_3/M_2Ox/SiO_2$. The predominant dehydrated surface MoOx species present for the model supported MoO_3/SiO_2 and multilayered supported $MoO_3/AlOx/SiO_2$, $MoO_3/ZrOx/SiO_2$, and $MoO_3/TiOx/SiO_2$ catalysts is the dioxo surface $O_2Mo(=O)_2$ species. The $\upsilon_s(Mo(=O)_2)$ vibration of the surface dioxo species varies from 981−1002 cm^{-1} for the different silica-supported catalysts. The slightly higher dioxo $\upsilon_s(Mo(=O)_2$ vibrations for the promoted systems are indicative of shorter Mo=O bond lengths for the surface modified SiO_2 caused by distortions from the interaction with the surface modifiers. This vibrational frequency also falls in the range exhibited for dehydrated surface MoOx on other oxide supports (990−1006 cm^{-1} for supported MoO_3/Al_2O_3, 980−997 cm^{-1} for supported MoO_3/ZrO_2, and 993−998 cm^{-1} for supported MoO_3/TiO_2)[3,74,77] and suggests that dioxo surface $O_2Mo(=O)_2$ species may also be the predominant species on these oxide supports.

4.2.4. Supported $WO_3/M_2Ox/SiO_2$. Whereas the major dehydrated surface WOx species on SiO_2 is the dioxo surface $O_2W(=O)_2$ species, it is transformed to predominantly monoxo surface $O_4W{=}O$ species in the presence of the surface M_2Ox species on SiO_2. The dioxo $\upsilon_s(W{=}O)_2$ vibrates at ∼985 cm^{-1} and monoxo $\upsilon_s(W{=}O)$ vibration appears between 1008−1020 cm^{-1}. The monoxo $\upsilon_s(W{=}O)$ vibrations on the surface modified SiO_2 fall in the range observed for dehydrated surface WOx on other oxide supports (1003−1020 cm^{-1} for supported WO_3/Al_2O_3, 1001−1015 cm^{-1} for supported WO_3/ZrO_2, and 1007−1016 cm^{-1} for supported WO_3/TiO_2)[3,77,93,94] and suggest that monoxo surface $O_4W{=}O$ species are the predominant surface tungstate species on non-SiO_2 supports, especially at higher surface coverage since the bands shift to higher wavenumber values with coverage.

4.2.5. Supported $Re_2O_7/M_2Ox/SiO_2$. The only dehydrated surface rhenia species on SiO_2 and surface modified SiO_2 is the trioxo surface $ORe(=O)_3$ species with the $\upsilon_s(Re(=O)_3$ vibration at 1002−1010 cm^{-1}. The trioxo $\upsilon_s(Re(=O)_3)$ vibrations fall in the range observed for dehydrated surface ReOx species on other oxide supports (1004−1015 cm^{-1} for supported Re_2O_7/Al_2O_3, 995−1009 cm^{-1} for supported Re_2O_7/ZrO_2, and 1005−1009 cm^{-1} for supported Re_2O_7/TiO_2) and suggest that the trioxo surface $ORe(=O)_3$ species are the only surface rhenia species on all oxide supports.

4.3. Molecular Structural Behavior of the Periodic Groups. The in situ Raman and UV−vis DRS results reveal distinct periodic trends regarding the molecular structural behavior of group 5−7 surface metal oxides supported on surface modified SiO_2 catalysts. The supported group 5 metal oxides (VOx, NbOx, TaOx) on the surface modified SiO_2 maintain the isolated monoxo surface structure and do not transform to either dioxo or trioxo surface functionality. Similarly, the supported group 7 metal oxide of rhenia exists as a trioxo $Re(=O)_3$ functionality and does not transform to dioxo or monoxo species on the surface modified SiO_2 supports. The group 6 supported metal oxides (CrOx, MoOx, WOx), however, terminate with both dioxo $M(=O)_2$ and monoxo $(M{=}O)$ functionality and the monoxo/dioxo ratio is affected by the surface M_2Ox additives. Thus, the monoxo/dioxo ratio of the group 6 surface M_1Ox species can be *tuned* with the addition of the surface M_2Ox ligands (AlOx, TiOx, and ZrOx).

5. Conclusions

The molecular and electronic structures of the supported group 5−7 metal oxides on SiO_2 were found to be affected by the introduction of surface AlOx, ZrOx, and TiOx species on the silica support. All the dehydrated supported M_1Ox catalysts on the native SiO_2 and the surface modified SiO_2 supports predominantly contain isolated surface M_1Ox species. The surface vanadia species maintain their monoxo structure both in the absence and presence of the surface modifiers. The dioxo/monoxo ratio of the supported group 6 metal oxides (CrOx and WOx) and the distortion of the dioxo surface MoOx species, however, were significantly influenced by the surface modifiers. The corresponding electronic structures of the supported group 6 metal oxides were also significantly changed by the presence of the surface modifiers (higher Eg values in the presence of the surface modifiers). The trioxo surface ReO_4 species, however, is not affected by the presence of the surface modifiers. The structural changes of the surface metal oxide species demonstrate that the group 5−7 supported transition metal oxides preferentially anchor to the surface modifiers (AlOx, ZrOx, and TiOx) than exposed silica sites of the support. These new insights can also assist in the structural determination of group 5−7 transition metal oxide-containing zeolites and molecular sieves (e.g., MOx/ZSM5, MOx/MCM-41, MOx/SBA15) and the establishment of molecular/electronic structure−activity/selectivity relationships in subsequent catalytic reaction studies.[45]

Acknowledgment. Funding was provided by the U.S. Department of Energy−Basic Energy Sciences (Grant No. DE-FG02-93ER14350).

References and Notes

(1) Wachs, I. E.; Segawa, K. In *Characterization of Catalytic Materials*; Wachs, I. E., Ed.; Butterworth-Heinemann: Boston, 1992; pp 69−88.
(2) Wachs, I. E. *Catal. Today* **2005**, *100*, 79.
(3) Wachs, I. E. *Catal. Today* **1996**, *27*, 437.
(4) De Boer, M.; Van Dillen, A. J.; Koningsberger, D. C.; Geus, J. W.; Vuurman, M. A.; Wachs, I. E. *Catal. Lett.* **1991**, *11*, 227.
(5) Jehng, J.-M.; Wachs, I. E. *Chem. Mater.* **1991**, *3*, 100.
(6) Busca, G.; Ramis, G.; Lorenzelli, V. *J. Mol. Catal.* **1989**, *50*, 231.
(7) Davydov, A. In *Molecular Spectroscopy of Oxide Catalyst Surfaces*; Sheppard, N. T., Ed.; Wiley: Hoboken, NJ, 2003.
(8) Haber, J. Crystallography of Catalyst Types. In *Catalysis: Science and Technology*; Boudart, M., Anderson, J. R., Eds.; Springer-Verlag: Berlin, 1981; Vol. 2, pp 13−95.
(9) Wachs, I. E. Molecular Structures of Surface Metal Oxide Species: Nature of Catalytic Active Sites in Mixed Metal Oxides. In *Metal Oxides: Chemistry and Applications*; Fierro, J. L. G., Heinemann, H., Eds.; CRC Taylor and Francis Press: Boca Raton, FL, 2005.
(10) Lee, E. L.; Wachs, I. E. *J. Phys. Chem. C* **2008**, *112*, 6487.
(11) Lee, E. L.; Wachs, I. E. *J. Phys. Chem. C* **2007**, *111*, 14410.
(12) Resini, C.; Montanari, T.; Busca, G.; Jehng, J. M.; Wachs, I. E. *Catal. Today* **2005**, *99*, 105.
(13) Oyama, S. T.; Went, G. T.; Lewis, K. B.; Bell, A. T.; Somorjai, G. A. *J. Phys. Chem.* **1989**, *93*, 6786.
(14) Banares, M. A.; Cardoso, J. H.; Agullo-Rueda, F.; Correa-Bueno, J. M.; Fierro, J. L. G. *Catal. Lett.* **2000**, *64*, 191.
(15) Moisii, C.; Deguns, E. W.; Lita, A.; Callahan, S. D.; van de Burgt, L. J.; Magana, D.; Stiegman, A. E. *Chem. Mater.* **2006**, *18*, 3965.
(16) Dines, T. J.; Inglis, S. *Phys. Chem. Chem. Phys.* **2003**, *5*, 1320.
(17) Groppo, E.; Damin, A.; Bonino, F.; Zecchina, A.; Bordiga, S.; Lamberti, C. *Chem. Mater.* **2005**, *17*, 2019.
(18) Groppo, E.; Lamberti, C.; Bordiga, S.; Spoto, G.; Zecchina, A. *Chem. Rev.* **2005**, *105*, 115.
(19) Gao, X.; Wachs, I. E. *J. Catal.* **2000**, *192*, 18.
(20) Gao, X.; Fierro, J. L. G.; Wachs, I. E. *Langmuir* **1999**, *15*, 3169.

(21) Gao, X.; Bare, S. R.; Fierro, J. L. G.; Wachs, I. E. *J. Phys. Chem. B* **1999**, *103*, 618.
(22) Reddy, B. N.; Subrahmanyam, M. *Langmuir* **1992**, *8*, 2072.
(23) Mariscal, R.; Galan-Fereres, M.; Anderson, J. A.; Alemany, L. J.; Palacios, J. M.; Fierro, J. L. G. *Environmental Catalysis*; Centi, G., et al.,Eds.; SCI: Rome, 1995; p 223.
(24) Amiridis, M. D.; Solar, J. P. *Ind. Eng. Chem. Res.* **1996**, *35*, 978.
(25) Wauthoz, P.; Machej, T.; Grange, P. *Appl. Catal.* **1991**, *69*, 149.
(26) Vogt, E. T. C.; Boot, A.; van Dillen, A. J.; Geus, J. W.; Janssen, F. J. J. G.; van den Kerkhof, F. M. G. *J. Catal.* **1988**, *114*, 313.
(27) Galan-Fereres, M.; Mariscal, R.; Alemany, L. J.; Fierro, J. L. G. *J. Chem. Soc., Faraday Trans.* **1994**, *90*, 3711.
(28) Santacesaria, E.; Sorrentino, A.; Tesser, R.; Di Serio, M.; Ruggiero, A. *J. Mol. Catal. A* **2003**, *204*−*205*, 617.
(29) Iannazzo, V.; Neri, G.; Galvagno, S.; Di. Serio, M.; Tesser, R.; Santacesario, E. *Appl. Catal., A* **2003**, *246*, 49.
(30) Quaranti, N. E.; Soria, J.; Cortes Corberan, V.; Fierro, J. L. G. *J. Catal.* **1997**, *171*, 1.
(31) McDaniel, M. P.; Welsh, M. B.; Dreiling, M. J. *J. Catal.* **1983**, *82*, 98.
(32) Conway, S. J.; Falconer, J. W.; Rochester, C. H. *J. Chem. Soc. Faraday Trans.* **1989**, *85*, 71.
(33) Rajagopal, S.; Grimm, T. L.; Collins, D. J.; Miranda, R. *J. Catal.* **1992**, *137*, 453.
(34) Henker, M.; Wendlandt, K. P.; Valyon, J.; Bornmann, P. *Appl. Catal.* **1991**, *69*, 205.
(35) Damyanova, S.; Docteva, A.; Vladov, C.; Petrov, L.; Grange, P.; Delmon, B. *Belg. Chem. Commun.* **1999**, *30*, 306.
(36) Damyanova, S.; Centeno, M. A.; Petrov, L.; Grange, P. *Spectrochim. Acta A* **2001**, *57*, 2495.
(37) Reddy, B. M.; Chowdhury, B.; Smirniotis, P. G. *Appl. Catal., A* **2001**, *211*, 19.
(38) Moulijn, J. A.; Mol, J. C. *J. Mol. Catal.* **1988**, *46*, 1.
(39) Mandelli, D.; van Vliet, M. C. A.; Arnold, U.; Sheldon, R. A.; Schuchardt, U. *J. Mol. Catal. A* **2001**, *168*, 165.
(40) Rajadhyaksha, R. A.; Hausinger, G.; Zeilinger, H.; Ramstetter, A.; Schmeiz, H.; Knözinger, H. *Appl. Catal.* **1989**, *51*, 67.
(41) Jehng, J.-M.; Wachs, I. E.; Weckhuysen, B. M.; Schoonheydt, R. A. *J. Chem. Soc. Faraday Trans.* **1995**, *91*, 953.
(42) Lapina, O. B.; Mastikhin, V. M.; Dubkov, K. A.; Mokrinski, V. V. *J. Mol. Catal.* **1994**, *87*, 57.
(43) Lakshmi, J. L.; Ihasz, N. J.; Miller, J. M. *J. Mol. Catal. A* **2001**, *165*, 199.
(44) Miller, J. M.; Lakshmi, L. J. *Appl. Catal., A* **2000**, *190*, 197.
(45) Lee, E. L.; Wachs, I. E. *J. Catal.* **2008**, *258*, 103.
(46) Gao, X.; Bare, S. R.; Fierro, J. L. G.; Banares, M. A.; Wachs, I. E. *J. Phys. Chem. B* **1998**, *102*, 5653.
(47) Gao, X.; Bare, S. R.; Weckhuysen, B. M.; Wachs, I. E. *J. Phys. Chem. B* **1998**, *102*, 10842.
(48) Jehng, J.-M.; Wachs, I. E. *J. Phys. Chem.* **1991**, *95*, 7373.
(49) Tian, H.; Wachs, I. E.; Briand, L. E. *J. Phys. Chem. B* **2005**, *109*, 23491.
(50) Mestl, G.; Srinivasan, T. K. K.; Knözinger, H. *Langmuir* **1995**, *11*, 3795.
(51) Weber, R. S. *J. Catal.* **1995**, *151*, 470.
(52) Brinker, C. J.; Kirkpatrick, R. J.; Tallant, D. R.; Bunker, B. C.; Montez, B. *J. Non-Cryst. Solids* **1988**, *99*, 418.
(53) McMillan, P. *Am. Mineral.* **1984**, *69*, 622.
(54) Galeener, F. L.; Mikkelsen, J. C., Jr. *Phys. Rev. B* **1981**, *23*, 5527.
(55) Galeener, F. L.; Geissberger, A. E. *Phys. Rev. B* **1983**, *27*, 6199.
(56) Morrow, B. A.; Mcfarlan, A. J. *J. Non-Cryst. Solids* **1990**, *120*, 61.
(57) Uchino, T.; Tokuda, Y.; Yoko, T. *Phys. Rev. B* **1998**, *58*, 5322.
(58) Yudaev, I. V.; Gan, Z.; Paukshtis, E. A.; Wachs, I. E.; Lapina, O. B., unpublished.
(59) Banares, M. A.; Cardoso, J. H.; Agullo-Rueda, F.; Correa-Bueno, J. M.; Fierro, J. L. G. *Catal. Lett.* **2000**, *64*, 191.
(60) Das, N.; Eckert, H.; Hu, H.; Wachs, I. E.; Walzer, J. F.; Feher, F. J. *J. Phys. Chem.* **1993**, *97*, 8240.
(61) Burcham, L. J.; Deo, G.; Gao, X.; Wachs, I. E. *Topics Catal* **2000**, *11/12*, 85.
(62) Went, G. T.; Oyama, S. T.; Bell, A. T. *J. Phys. Chem.* **1990**, *94*, 4240.
(63) Deo, G.; Wachs, I. E. *J. Catal.* **1994**, *146*, 323.
(64) Dobler, J.; Pritzsche, M.; Sauer, J. *J. Am. Chem. Soc.* **2005**, *127*, 10861.
(65) Magg, N.; Immaraporn, B.; Giorgi, J. B.; Schroeder, T.; Baumer, M.; Dobler, J.; Wu, Z.; Kondratenko, E.; Cherian, M.; Baerns, M.; Stair, P. C.; Sauer, J.; Freund, H. J. *J. Catal.* **2004**, *226*, 88.
(66) Avdeev, V. I.; Zhidomirov, G. M. *Res. Chem. Intermed.* **2004**, *30*, 41.
(67) Weckhuysen, B. M.; Wachs, I. E. *J. Phys. Chem. B* **1997**, *101*, 2793.
(68) Kim, D. S.; Wachs, I. E. *J. Catal.* **1993**, *142*, 166.
(69) Vuurman, M. A.; Wachs, I. E.; Stufkens, D. J.; Oskam, A. *J. Mol. Catal.* **1993**, *80*, 209.
(70) De Boer, M.; Van Dillen, A. J.; Koningsberger, D. C.; Geus, J. W.; Vuurman, M. A.; Wachs, I. E. *Catal. Lett.* **1991**, *11*, 227.
(71) Busca, G. *J. Raman Spectrosc.* **2002**, *33*, 348.
(72) Cornac, M.; Janin, A.; Lavalley, J. C. *Polyhedron* **1986**, *5*, 183.
(73) Williams, C. C.; Ekerdt, J. G.; Jehng, J.-M.; Hardcastle, F. D.; Turek, A. M.; Wachs, I. E. *J. Phys. Chem.* **1991**, *95*, 8781.
(74) Hu, H.; Wachs, I. E.; Bare, S. R. *J. Phys. Chem.* **1995**, *99*, 10897.
(75) Banares, M. A.; Hu, H.; Wachs, I. E. *J. Catal.* **1994**, *150*, 407.
(76) Chempath, S.; Zhang, Y.; Bell, A. T. *J. Phys. Chem. C* **2007**, *111*, 1291.
(77) Vuurman, M. A.; Wachs, I. E. *J. Phys. Chem.* **1992**, *96*, 5008.
(78) Kim, D. S.; Ostomecki, M.; Wachs, I. E.; Kohler, S. D.; Ekerdt, J. G. *Catal. Lett.* **1995**, *33*, 209.
(79) Vuurman, M. A.; Stufkens, D. J.; Oskam, A. *J. Mol. Catal.* **1992**, *76*, 263.
(80) Kim, D. S.; Wachs, I. E. *J. Catal.* **1993**, *141*, 419.
(81) Beattie, I. R.; Ozin, G. A. J. Chem. Soc. A, 1969, *2615*.
(82) Hardcastle, F. D.; Wachs, I. E.; Horsley, J. A.; Via, G. H. *J. Mol. Catal.* **1988**, *46*, 15.
(83) Weckhuysen, B. M.; Verberckmoes, A. A.; De Baets, A. R.; Schoonheyde, R. A. *J. Catal.* **1997**, *166*, 160.
(84) Weckhuysen, B. M.; Wachs, I. E.; Schoonheydt, R. A. *Chem. Rev.* **1996**, *96*, 3327.
(85) Hardcastle, F. D.; Wachs, I. E. *J. Raman Spectrosc.* **1990**, *21*, 683.
(86) Jorgensen, J. D.; Hu, Z.; Teslic, S.; Argyriou, D. N.; Short, S.; Evans, J. S. O.; Sleight, A. W. *Phys. Rev. B* **1999**, *59*, 215.
(87) Wells, A. *Structural Inorganic Chemistry*; Oxford University: London, 1984.
(88) Ostromecki, M. M.; Burcham, L. J.; Wachs, I. E. *J. Mol. Catal. A* **1998**, *132*, 59.
(89) Turek, A. M.; Wachs, I. E.; DeCanio, E. *J. Phys. Chem.* **1992**, *96*, 5000.
(90) Sanderson, R. T. *J. Chem. Educ.* **1988**, *65*, 112.
(91) Jehng, J.-M.; Deo, G.; Weckhuysen, B. M.; Wachs, I. E. *J. Mol. Catal. A* **1996**, *110*, 41.
(92) Weckhuysen, B. M.; Jehng, J.-M.; Wachs, I. E. *J. Phys. Chem. B* **2000**, *104*, 7382.
(93) Vuurman, M. A.; Wachs, I. E.; Hirt, A. M. *J. Phys. Chem.* **1991**, *95*, 9928.
(94) Kim, D. S.; Ostromecki, M.; Wachs, I. E. *J. Mol. Catal. A* **1996**, *106*, 93.

JP805265M